MAGNETOELASTIC WIRELESS SENSING OF TISSUE GROWTH FOR SELF-EXPANDING BILIARY STENTS

Mark T. Richardson[1*], Scott R. Green[2], Yogesh B. Gianchandani[1,2]
[1]*Department of Electrical Engineering and Computer Science, University of Michigan, Ann Arbor*
[2]*Department of Mechanical Engineering, University of Michigan, Ann Arbor*

ABSTRACT

Tissue growth in biliary stents causes a loss of patency after only 2-12 months in 50% of cases, leading to complications such as jaundice or cholangitis. We report micro-machined resonant magnetoelastic sensors for monitoring tissue growth on biliary stents and an appropriate transmit/receive coil configuration for these sensors. An 8 mm diameter stainless steel mesh that was used as a self-expanding stent had a 33% recovery expansion in the absence of loading. Paraffin mass loads up to 251 mg simulated tissue growth on 37.5x2 mm^2, 28 μm thick sensors. A resonant frequency shift from 57.85 kHz to 22.35 kHz was observed. Varying the local viscosity over the range of healthy and diseased bile gave a shift of 1 kHz. The sensor response without mounting in the stent was negligibly different.

I. INTRODUCTION

Stents are used to maintain the patency of a variety of vessels and ducts to relieve high blood pressure and other symptoms. One example is the bile duct that connects the liver, gall bladder, pancreas and small intestine, and transports bile for digestion. Restricted flow is often caused by a constriction due to pancreatitis, cholangitis, cancerous tumors, or gallstones. Unfortunately, stent placement often results in significant tissue growth and loss of patency in 50% of cases after 2-12 months [1,2]. An accumulation of 'sludge' precedes the tissue growth, increasing the viscosity of bile [3,4]. Intervention such as stent replacement is often required when symptoms of blockage recur.

Current techniques for indirectly diagnosing a blockage use a blood test to monitor enzymes such as bilirubin and alkaline phosphatase, etc. Computed tomography imaging of the duct is then used to confirm there is a stricture. A direct method such as in Fig. 1 would help to monitor tissue growth (or associated parameters) and enable timely intervention while eliminating unnecessary procedures.

We have previously reported on micro-electro-discharge machining of cardiac stents and their use as inductors coupled to capacitive pressure sensors for sensing blood pressure and flow [5]. Cardiac stents are deployed by balloon angioplasty, and undergo a plastic deformation. In contrast, biliary stents are deployed by endoscopic retrograde cholangiopancreatography or percutaneous transhepatic cholangiography and normally rely on elastic self-expansion. The bile duct requires stents that are typically twice the diameter (8 mm vs 4 mm) and structurally different.

Past work in magnetoelastic sensors has demonstrated the feasibility of sensing mass loading, media viscosity, and other properties in environmental/industrial applications [6,7]. These are resonant magnetoelastic devices that respond to an interrogative magnetic field in its basal plane. As the device vibrates, its magnetostrictive properties result in the generation of a magnetic field. This field can be detected wirelessly with a pickup coil and frequency information can be extracted. Changes in the resonant frequency are correlated to changes in the local environment of the sensor. Tissue growth in the bile duct can be considered a mass loading effect, while mucal precursors increase viscosity. Thus the sensors provide a direct measure of key parameters. However, several critical challenges must be addressed.

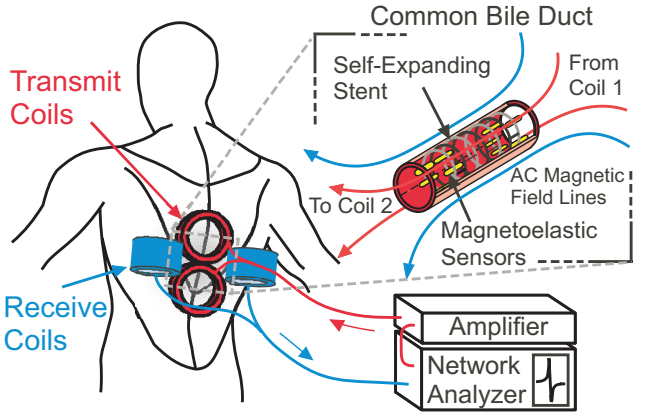

Fig. 1: Conceptual diagram of magnetoelastic sensing of tissue growth for billiary stents.

II. DESIGN AND FABRICATION

The diagram in Fig. 1 outlines the method for wirelessly sensing tissue growth in a biliary stent. A network analyzer controls an amplifier, driving the transmit coils in an AC frequency sweep that produces a corresponding magnetic field sweep. The sensors, which are integrated into the stent, resonate at a mass-loading dependent frequency and are detected by the receive coils. As will be explained in section IV, this configuration utilizes local null-points of the transmit signal, improving the resolution of the receive coils, and allowing the oscillating field to be directed appropriately along the length of the sensors. Positioning of the coils on the back was chosen because there tends to be less variation in intervening tissue thickness from person to person.

Commercial self-expanding stents (Boston Scientific, Natick, MA USA) rely on elastic expansion of a woven metal mesh. For this work, various planar 304 stainless steel meshes were rolled into a tubular shape and woven together at the seam. By using a planar topology, other materials, shapes, and structures can be micro-machined.

*Corresponding Author: mtrichar@umich.edu 1301 Beal, Ann Arbor, MI 48109-2122, USA

$$E_{eff}\frac{(d+2t_{tis})}{1-\nu_p^{\,2}}\frac{\partial}{\partial x}\left(w(x)\frac{\partial u}{\partial x}\right)-\underbrace{\left(\rho w(x)d+1.98w(x)\rho_{fl}\sqrt{\frac{2\nu}{\omega}}+2\rho_{tis}w(x)t_{tis}\right)}_{\text{Mass Loading Terms}}\frac{\partial^2 u}{\partial t^2}-\underbrace{2w(x)\mu\sqrt{\frac{\omega}{2\nu}}}_{\text{Viscous Damping Term}}\frac{\partial u}{\partial t}+\frac{\partial}{\partial x}\underbrace{\left[\frac{G_{tis}}{\omega}(2t_{tis})w(x)\frac{\partial^2 u}{\partial x\partial t}\right]}_{\text{Hysteretic Damping Term}}=-\frac{\partial}{\partial x}\left(Edw(x)\underbrace{\lambda(t,x)}_{\substack{\text{Magnetostrictive}\\ \text{Coupling Term}}}\right) \quad (1)$$

Table 1 Equation 1 Parameters

$E_{eff} \equiv$ Effective Young's Modulus $= \frac{Ed+2E_{tis}t_{tis}}{d+2t_{tis}}$	d = Sensor Thickness
ν = Fluid Kinematic Viscosity	t_{tis} = Tissue Thickness
υ = Local Sensor Displacement	w(x) = Sensor Width
ω = Input Signal Radial Frequency	ρ = Sensor Density
E = Sensor Young's Modulus	ρ_{fl} = Fluid Density
E_{tis} = Tissue Young's Modulus	ρ_{tis} = Tissue Density
ν_p = Sensor Poisson's Ratio	G_{tis}=Tissue Loss Modulus

The stent and sensor combination is compressed into a small sleeve which is retracted on deployment, allowing the stent to expand against the constricted duct. Since the area of constriction is positioned mid-length of the stent, the sensor is also attached here. The sensor is positioned along the stent sidewall so as not to exacerbate the duct occlusion.

The 37.5x2 mm^2 magnetoelastic sensors are patterned from planar Ni/Fe foil (Metglas™ 2826MB) by μEDM [8,9]. After bonding to a wire with cyanoacrylate, the wire is looped into the middle of the stent mesh. These stent and sensor prototypes provide an indication of the importance of stent material, pattern density, and sensor support conditions in the determination of signal strength and sensor saturation limits. The use of biocompatible adhesive and the addition of a parylene coating would improve the biocompatibility of future designs.

III. MAGNETOELASTIC SENSOR MODELING

In our proposed application, a dynamic biological environment affects the magnetoelastic sensor. Specifically, the surrounding liquid medium along with cell epithelialization and sludge accumulation has direct effects on the response of the sensor, in terms of both resonant frequency and signal amplitude. To better quantify these effects and to provide insight into the transduction technique, a mathematical model is proposed and utilized. For the following study, the sensor length is assumed to be along the x-axis. Also, the sensor is assumed to be fixed only at the exact mid-length, resulting in free-free end conditions.

The equation of motion (Eq. 1) relating the input magnetic fields to resulting sensor displacement is derived using Newton's Law and is shown above. The parameters are defined in Table 1.

Tissue density is approximated as that of water, while moduli are from [10]. The first and third mass loading terms are simply the mass per unit length of the sensor and tissue, respectively. This assumes a uniform layer of tissue growth on both sides of the sensor. The second mass loading term is an effective mass loading provided by the surrounding viscous fluid, as described in [11]. Briefly, the sensor surface and fluid interact, and a certain amount of the fluid – with a characteristic length dependent on the activation frequency and fluid viscosity – is activated and contributes to the kinetic energy of the vibration. Also, as described in [11], the surrounding fluid provides a damping mechanism due to viscous shear stresses. From [12] and [13], a viscoelastic material, such as tissue, undergoing vibrations can be modeled as having a real and complex Young's modulus, with the complex modulus being incorporated into the equation of motion as shown in the hysteretic damping term. As described in [14] and [15], the strain of amorphous metals can be related to the applied magnetic field as follows:

$$\lambda(t,x)=\frac{3\lambda_s}{2}\left(\frac{H_{eff}(t,x)^2}{H_a^{\,2}}-\frac{1}{3}\right) \quad (2)$$

In equation (2), λ_s is the magnetostrictive coefficient, and is ~12ppm for Metglas™ 2826MB. Also,

$$H_{eff}(t,x)=\left(H_{DC}+H_{AC}\cos(\omega t)\right)\psi(x) \quad (3)$$

where H_{DC} is the applied DC magnetic field strength, H_{AC} is the applied AC magnetic field strength, and $\Psi(x)$ is a shape function that arises due to edge effects at the sharp discontinuity in permeability at the sensor/fluid interface. For the purposes of this study, the shape function is determined by fitting a curve to numerical results calculated with FEA. In equation (3), H_a is the anisotropy field of the sensor, which may be dependent on sensor material, sensor processing conditions, and sensor length-to-width aspect ratio. We assume that the necessary applied DC biasing field is equal to the anisotropy field, and the AC field is some proportion of the anisotropy field. This removes any dependence of the solution on the numerical value of the difficult to characterize anisotropy field.

The equation of motion and associated boundary conditions can be solved via the method of eigenfunction expansion as described in [16]. The result is an infinite summation of eigenfunctions multiplied by time-dependent functions related to the mass loading terms, damping terms, stiffness terms, and applied magnetic field. Because we are generally concerned with only the first resonant frequency of the system, a one-term approximation is appropriate and justified according to a truncation analysis.

Figure 2 shows the amplitude of the displacement of the sensor tip versus frequency for two different tissue thicknesses and two different representative fluids.

IV. EXPERIMENTAL RESULTS

The test setup is diagramed in Fig. 3. As can be seen with the AC magnetic field lines, the coils are configured such that the transmit and receive coils can both couple to the sensor, but not with each other. Since the sensor is relatively close to the coils, it acts similar to a dipole, with field lines emanating in a circular path from one end to the other. The receive coils are located at a null point of the transmit coils and are oriented perpendicular to the direction of the transmit field but in-line with the sensor's field. Note that maximum signal comes when the field lines match up with the longitudinal axis of the sensor. Aligning the coils directly along the sensor's axis is not possible because the

bile duct runs almost vertically, and the sensor must as well.

Figure 4 shows a self-expanding stainless steel mesh stent at the edge of a tube with 33% expansion from the deliverable diameter. The spring constant was typically 13.32 mN/μm when compressed and 3.01 mN/μm after expansion. Note that commercial self-expanding stents (Boston Scientific, Natick, MA USA) are made from Nitinol wire mesh - a nickel titanium alloy with double the yield stress of stainless steel - and are therefore capable of larger expansions. Figure 5 shows a stent with a mounted sensor. The 3 mm thick paraffin coating on the sensor simulates the mass loading due to tissue growth.

In order to ensure that the signals transmitted and received by the system and sensor were sufficient, a vial containing the device under test and fluids representative of bile was packaged in a 7.5 cm thick homogeneous mixture of bovine tissue (ground beef). This was meant to simulate the amount of flesh between the bile duct and the transmit/receive coils. Since the magnetoelastic sensor requires a DC magnetic field as well as the AC field, neodymium permanent magnets were attached at both ends of the vial.

Viscosities spanning those of bile with varying sludge content are from 1-14 cP. The viscosity of the test fluid was varied from 0 to 16 cP by adding measured amounts of sucrose to DI water. Unattached 37.5x2 mm^2 sensors were used to control the effects of mass loading and stent interference. The resonant frequency of the magnetoelastic sensors typically shifted by a total of 1 kHz (Fig. 6). This demonstrates sensitivity to viscosity shifts that precede tissue growth.

To simulate tissue growth (Fig. 7), sensors were successively dipped in paraffin and tested in 20% sucrose water (~2.5 cP). Unattached sensors were used to isolate any effects from the stent. As more mass was added, the typical values of the resonant frequency shifted from 57.45 kHz down to 22.475 kHz with 161.5 mg added. Curves from sensors immersed in fluids of different viscosities very nearly overlaid this plot, indicating the sensors are much more sensitive to the clinically important parameter of tissue growth.

Mass loading from tissue growth was emulated within a mesh stent (Figs. 5,7) to determine if there was any interference from a potential faraday cage or from physical contact between the sensor and stent. The sensors were removed, dipped in paraffin, and remounted in the same location for each data point. The mounted sensors behaved very similar to the unattached sensors, but the added stiffness of the wire support shifted the frequency slightly higher. The sensors typically resonated around 22.35 kHz with a mass loading of 251 mg. The frequency response of the sensor model from the previous section was also plotted for both simulated tissue and paraffin mass loading (Fig. 7). The model closely follows the trends of the experimental data but with an offset.

Asymmetric paraffin mass loading was tested on 37.5x6 mm^2 sensors. The sensor had similar normalized frequency shifts when mass was added to only one end and when mass

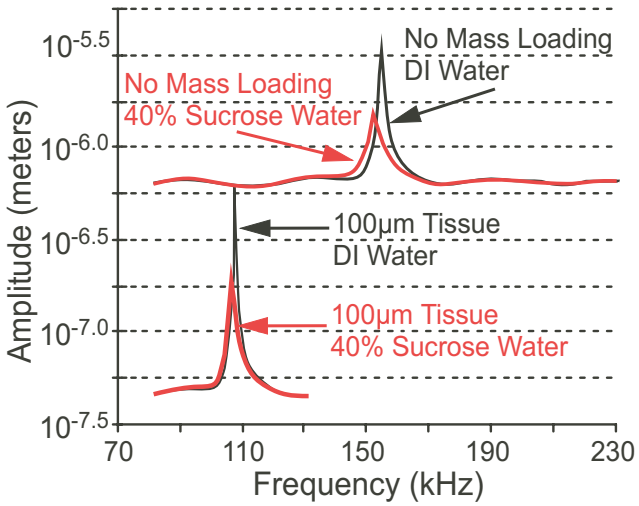

Fig. 2: Model simulation of a 12.5 mm magnetoelastic sensor displacement frequency response for various loading conditions.

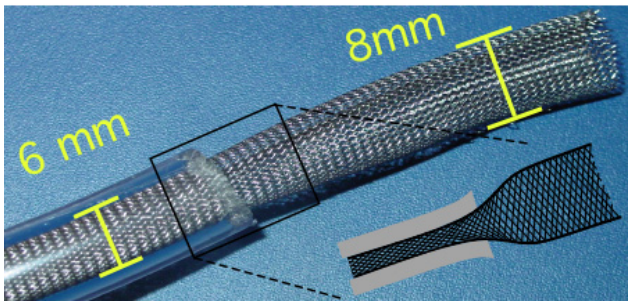

Fig. 4: As the stent expands 33% from the deliverable diameter, the longitudinal links rotate to align with the circumference.

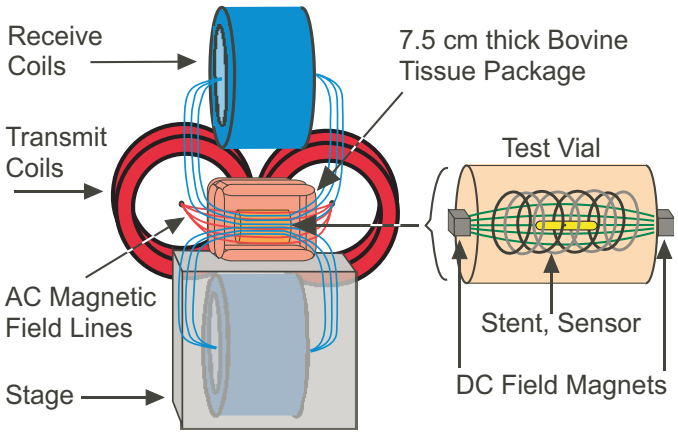

Fig. 3: Magnetoelastic sensor test setup features a test vial with viscous fluid (0-16 cP) and a 7.5 cm thick bovine tissue package to simulate the body environment. Permanent magnets on the vial bias the sensor, transmit coils excite the sensor with an AC magnetic field, and the receive coils sense the resonant frequency.

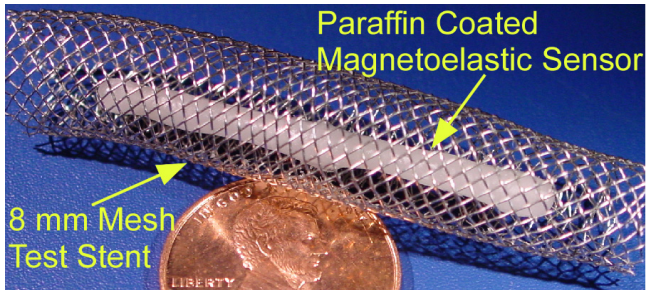

Fig. 5: Magnetoelastic sensor mounted in an 8 mm x 50 mm stainless steel mesh test stent after 251 mg paraffin loading.

was added symmetrically (Fig. 8) on both ends. The potential for non-uniform tissue growth affecting the sensor response is thus a lesser concern.

V. DISCUSSION

There are still several improvements under investigation. Biocompatibility issues must be addressed more rigorously. Corrosion of Metglas™ and permanent magnets in an aqueous environment is the most important issue although coatings have been claimed to resolve the problem [17]. If possible, the DC magnetic field bias should be incorporated into the stent to eliminate the need for magnets external to the implant.

Sensor contact with the stent is a concern under certain circumstances as the contact would add nonlinearity to the sensor response and degrade the signal. One area for further investigation is whether tissue growth could bind the sensor against the stent wall. As the sensor length is scaled down this becomes less of a concern. Another option is to explore structural variation to prevent contact.

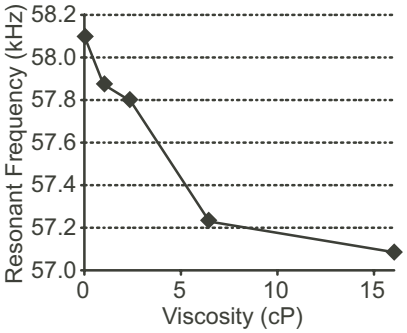

Fig. 6: Resonant frequency response due to increasing viscosity in the range of sludge in the bile duct. As viscosity increases, tissue is more likely to form on the surface of the stent.

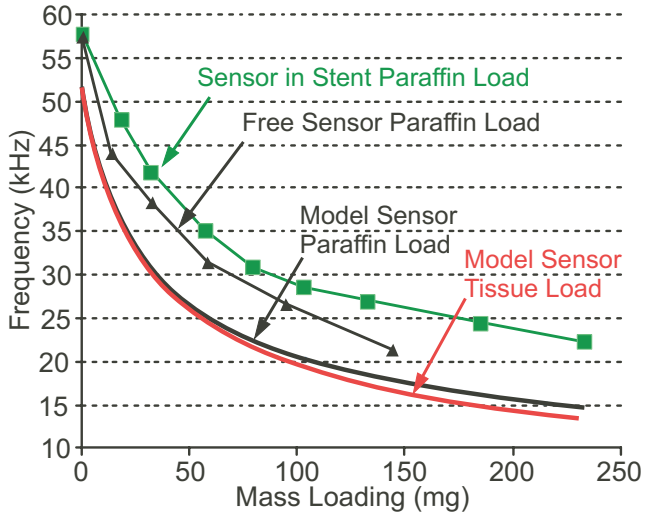

Fig. 7: Theoretical and experimental paraffin and tissue mass loading responses. Mounted magnetoelastic sensors were in an 8 mm diameter stainless steel mesh stent.

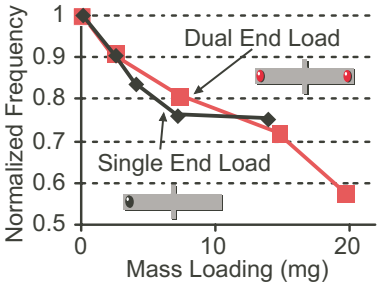

Fig. 8: Non-uniform paraffin mass loading simulates uneven tissue growth. The similar response suggests this type of loading is a lesser concern.

V. CONCLUSION

A tissue-growth-monitoring sensor for biliary stents was investigated. Planar self-expanding stents allow for integration of sensors and new materials. A stainless steel mesh stent expanded 33% from its deliverable diameter. At least 10x the initial mass of the 37.5x2 mm^2, 28 μm thick sensor can be added before the sensor saturates, and the resonant magnetoelastic response spans 40 kHz. These sensors could potentially be used in many types of stents to help wirelessly characterize their patency.

ACKNOWLEDGEMENTS

The authors acknowledge Dr. Grace Elta and Dr. Richard Kwon for discussions regarding stent usage and Ms. Farah Shariff for assistance with experiments. Metglas Inc. provided samples for this project. This work was supported in part by a National Science Foundation Graduate Research Fellowship, the NSF ERC for Wireless Integrated Microsystems (WIMS), and the University of Michigan.

REFERENCES

[1] B.H. Lee et. al., "Metallic Stents in Malignant Biliary Obstruction: Prospective Long-Term Clinical Results," *Am. J. Roentgenology*, 168 (3), pp. 741-745, 1997.

[2] J. Lee, J. Leung, "Long-Term Follow-up after Biliary Stent Placement for Postoperative Bile Duct Stenosis," *Gastrointestinal Endoscopy,* 54(2), pp. 272-274, 2001.

[3] H. Zhang et al., "Role of Bile Mucin in Bacterial Adherance to Biliary Stents," *J. Lab Clin Med*, 139(1), pp. 28-34, Jan 2002.

[4] M. Peng et al., "Studies of Sulfonated Polyethylene for Biliary Stent Application," *J. Appl. Polymer. Sci.*, 92, pp. 2450-2457, 2004.

[5] K. Takahata et al., "A Wireless Microsensor for Monitoring Flow and Pressure in a Blood Vessel Utilizing a Dual Inductor Antenna Stent and Two Pressure Sensors," *IEEE MEMS 2004*, pp. 216-219.

[6] M. Jain et al., "Magnetoelastic Microsensors for Environmental Monitoring," *IEEE MEMS 2001*, pp. 278-81.

[7] M. Jain, Q. Cai, C. Grimes, "A Wireless Micro-sensor for Simultaneous Measurement of pH, Temperature, and Pressure," *Smart Materials and Structures*, Vol. 10, 2001, pp. 347-353.

[8] T. Masaki et al., "Micro Electro-Discharge Machining and Its Applications," *IEEE MEMS '90*, pp. 21-26, 1990.

[9] K Takahata, YB Gianchandani, "Batch Mode Micro-Electro-Discharge Machining," *J.MEMS* 11(2), pp. 102-110, 2002.

[10] Y.C. Fung, *Biomechanics: Mechanical Properties of Living Tissues*. New York: Springer-Verlag, 1981. pp. 183.

[11] C. M. Darvennes, S.J. Pardue, "Boundary effect of a viscous liquid on a longitudinally vibrating bar: Theory and application," *J. Acoust. Soc. Am.*, 110(1), July 2001, pp. 216-224.

[12] P. L. Gatti and V. Ferrari, *Applied Structural and Mechanical Vibrations: Theory, Methods, and Measuring Instrumentation*, New York: E & FN Spon, 1999.

[13] S. Sorrentino, S. Marchesiello, and B. A. D. Piombo, "A new analytical technique for vibration analysis of non-proportionally damped beams," *J. Sound and Vib.*, 265(4), Aug 2003, pp. 765-82.

[14] M. Dapino et al., "Active and structural strain model for magnetoelastic transducers," *Proc. SPIE*, 3329, Jul 1998, pp. 198-209.

[15] J. D. Livingston, "Magnetomechanical Properties of Amorphous Metals," *Phys. Stat. Sol. (a)* 70, 1982. pp. 591-596.

[16] R. Haberman, *Applied Partial Differential Equations with Fourier Series and Boundary Value Problems*. 4th ed. Pearson

[17] M. Wilson et al "Corrosion of Intra-Oral Magnets in the Presence and Absence of Biofilms of Streptococcus Sanguis," *Biomaterials*, 16(9) 721-5, 1995.